Throughput and Coverage Analysis of a Multi-Element Broadband Fixed Wireless Access (BFWA) System in the Presence of Co-Channel Interference

Y. Q. Bian and A. R. Nix

Centre for Communications Research (CCR), University of Bristol,
Woodland Rd, Bristol, BS8 1UB, UK

{y.q.bian; andy.nix}@bristol.ac.uk

***Abstract*—This paper uses a detailed site-specific channel model to analyze the impact of path loss and Co-Channel Interference (CCI) in a multi-basestation Broadband Fixed Wireless Access (BFWA) network. The basestations are deployed in an urban setting and make use of sectorised multi-element arrays to suppress CCI from other cells/sectors. Customer Premises Equipment (CPE) is mounted at rooftop level on a number of surrounding buildings. Spatially correlated Multiple Input Multiple Output (MIMO) channels are produced for each link using channel data generated from the ray-tracing model. The tool predicts MIMO correlation based on radiowave propagation and antenna array geometries. The paper considers the use of Uniform Linear Arrays (ULA) and Uniform Circular Arrays (UCA) with a number of different element spacings. The results provide a unique insight into the deployment of multi-element WiMAX networks in an urban setting.**

Keywords- WiMAX, CCI, MIMO, ray tracing

I. INTRODUCTION

Broadband Fixed Wireless Access (BWA) is seen as an efficient way to meet the escalating business demands for high-speed symmetric internet connectivity. WiMAX promises to deliver high data rates over extensive areas to large numbers of users in the near future. The radio channel linking the basestation (BS) to the Customer Premises Equipment (CPE) is complex; especially in urban environments where line-of-sight cannot be guaranteed. Multiple Input Multiple Output (MIMO) radio systems have the ability to exploit such complex radio channels. The IEEE 802.16 WiMAX standard allows the deployment of wireless-MAN under non-line-of-sight (NLoS) radio conditions [2], The standard enables differentiated broadband services in the 2-11 GHz band using a range of channel bandwidths. The WiMAX Forum has identified several frequency bands for initial IEEE 802.16d deployments. This includes licensed (i.e. 2.5~2.69 and 3.4~3.6 GHz) and unlicensed spectrum (5.725~5.850 GHz). Three different physical (PHY) layer air-interfaces are defined [1] in the standard: 1) WirelessMAN-SC, 2) WirelessMAN-OFDM and 3) WirelessMAN-OFDMA. The OFDM PHY (using 256 carriers) is favored by the vendor community for high throughput fixed residential access [2].

In a multi-BS deployment it is vital to mitigate the harmful effects of Co-Channel Interference (CCI). This is necessary to achieve a high Quality of Service (QoS) and to enhance the resulting spectrum efficiency. It is important to note that the CCI has a direct impact on the frequency reuse plan.

Basic IEEE802.16 WiMAX performance results were presented in [2] and [3] using standard 3GPP and COST 231 channel models. Currently the SUI (Stanford University Interim) channel models [4] are widely used to represent the radio channel in a fixed WiMAX deployment. These models already include a Spatially Correlated Model (SCM) for SIMO channels. Unfortunately, statistical models of this type make a number of general assumptions that are not always met in practice. To overcome this limitation, in this paper we use a ray-tracing tool [5] to model the radio channel between a number of BS and their associated CPEs. In particular, we determine the multipath components (in terms of complex field, time of flight, and double directional spatial information) between *all* BSs and CPEs. Using this data set (together with a radio resource allocation plan), we then compute and analyse the resulting CCI for a Frequency Division Duplex (FDD) system.

Sectorised arrays are used at the BS to reduce the impact of CCI. These are particularly effective when the co-channel signal is spatially independent of the wanted signal. MIMO is also applied at the BS (on a per-sector basis) and CPE. The resulting MIMO correlation matrices are analyzed for a number of practical array geometries and deployment scenarios. At the BS we use three sectors. For each sector, a number of horizontally spaced MIMO elements are deployed, each with a 120^0 azimuth beamwidth. At the CPE we consider two cases: 1) a single omni antenna, and 2) a number of horizontally spaced 30^0 azimuth beamwidth elements.

The IEEE 802.16 standard defines seven combinations of modulation and coding rate. These are used to trade-off link speed against receiver sensitivity. Weaker channels therefore make use of slower link speeds (and vice versa). Adaptive Modulation and Coding (AMC) is considered in this paper to maximize the throughput of each individual link. Results demonstrate that good geographic coverage can be achieved in a dense urban environment. The use of BS sectorisation helps to suppress CCI, and results show that this is important at the higher link speeds (which are often interference limited).

The paper is organized as follows: section II explains the channel processing applied to the ray tracing data. Section III analyses the site specific channel data and compares it against the SUI reference model. Throughput and coverage results are presented in section IV for a multi-BS network deployment. Finally conclusions are drawn in section V.

II. SITE-SPECIFIC CHANNEL MODELLING

Complex Impulse Response (CIR) data is generated on a point to point basis using an outdoor ray tracing tool [5] at 3.5 GHz. The ray tracing model traces electromagnetic waves in 3D space and takes into account individual buildings, trees, corner

and roof-top edges, terrain blocking and scattering. The raw Multi-Path Component (MPC) data is created using isotropic element patterns. Specific element patterns are spatially convolved with the raw data in a later processing stage.

Fig.1 shows the structure of the channel generator (which is used to process the raw ray-tracing data). In a multi-BS environment, each CPE must be assigned to a most likely BS. We assume that the CPE connects to the BS with the strongest predicted power level. The strongest MPC component is then identified for each of the BS-CPE links. The most appropriate BS sector to serve each CPE is determined from the Angle of Departure (AoD) of the strongest MPC. The Angle of Arrival (AoA) of the strong MPC is used to orientate the directional CPE antenna, as shown in Fig. 2. It should be noted that in NLoS, the CPE may actually be orientated in the direction of a strong MPC, and not directly towards the serving sector. The ETSI specific antenna beam patterns (with side lopes) [6] are then spatially convolved onto the isotropic ray tracing generated CIR data.

For each BS-CPE link in the network we now have detailed CIR information (i.e. the complex field, time of flight, AoA and AoD of each MPC). Together with the BS and CPE array geometries, we now expand this point source SISO data to derive a set of MIMO channel matrices. This SISO to MIMO expansion is performed as part of the Ray-Tracing Deterministic MIMO (RTD-MIMO) model shown in fig. 1.

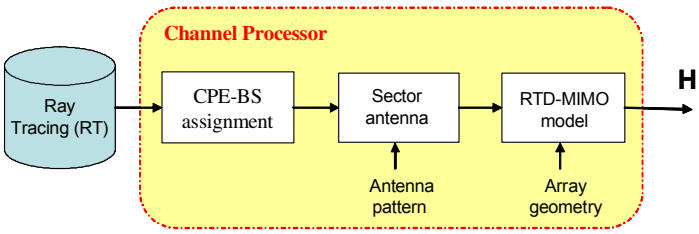

Figure 1. MIMO Channel Genaration from raw Ray-Tracing data

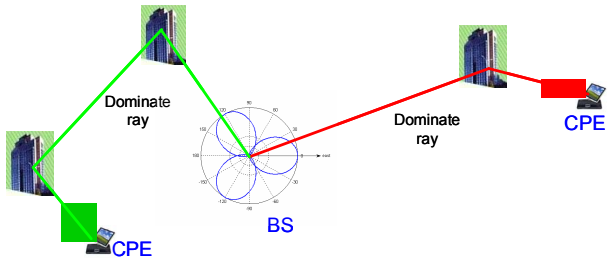

Figure 2. Concept of CPE-BS-sector assignment

Within the RTD-MIMO model, the following five procedures are performed,

1. Apply a random phase $\Delta\theta_q$ to the complex field of each point source MPC;
2. Generate the MIMO H-matrix for each MPC based on knowledge of the [m,n] array geometries;
3. Apply time binning to the [m,n]-th H-matrix data set based on the system bandwidth (e.g., 5 or 10 MHz). MPCs in the same time bin are vector combined;
4. Fourier transform each CIR to generate the [m,n]-th frequency response at each of the 256 OFDM sub-carriers;
5. Repeat steps 1-4 to achieve a statistically large set of channel realisations.

Generally, MIMO spatial correlation results from both the radio propagation characteristics (i.e. narrow angle spreads) and the MIMO antenna array geometries (i.e. narrow element spacings). Of the simple antenna array configurations, the Uniform Linear Array (ULA) is the most common form employed in cellular and personal communication systems [7]. Recently, there has been increased interest in the use of Uniform Circular Arrays (UCA). For simplicity, we place the MIMO arrays in the horizontal plane and only consider azimuth angles in the propagation geometry. Assuming N transmit antennas and M receive antennas, the antenna array vectors at the BS and CPE can be written as:

$$\mathbf{v}_{tx} = [v_{tx}(1), \quad \cdots, \quad v_{tx}(n), \quad \cdots, \quad v_{tx}(N)] \tag{1}$$

$$\mathbf{v}_{rx} = [v_{rx}(1), \quad \cdots, \quad v_{rx}(m), \quad \cdots, \quad v_{rx}(M)] \tag{2}$$

where the $v_{tx}(n)$ and $v_{rx}(m)$ denote the antenna elements for the n-th transmit antenna and m-th receive antenna.

For the ULA case, v_{tx} and v_{rx} in equations (1) and (2) represent antenna separations relative to the point source ray departure/arrival point. Assuming ideal plane waves at the BS and CPE array, we can compute the complex field phase offsets at the tx (BS) and rx (CPE) associated with the relative displacement of each MIMO element. For the q-th MPC we can write:

$$\Delta\beta_{tx}^{q}(n) = 2\pi \frac{v_{tx}(n)}{\lambda} \sin\left(\alpha_{AoD}^{q}\right) \tag{3}$$

$$\Delta\beta_{rx}^{q}(m) = 2\pi \frac{v_{rx}(m)}{\lambda} \sin\left(\alpha_{AoA}^{q}\right) \tag{4}$$

where α_{AoD}^{q}, α_{AoA}^{q} and λ represent the AoD and AoA in the azimuth plane for the q-th MPC, and the wavelength respectively.

For a UCA the antenna elements lie on a circle of radius R. The v_{tx} and v_{rx} terms include the deployment angle of each array element with regards to the horizontal axis at the BS and CPE. The phase shifts for the q-th MPC at the BS and CPE are given by:

$$\Delta\beta_{tx}^{q}(n) = 2\pi \frac{R}{\lambda} \cos(v_{tx}(n) - \alpha_{AoD}^{q}) \tag{5}$$

$$\Delta\beta_{rx}^{q}(m) = 2\pi \frac{R}{\lambda} \cos(v_{rx}(m) - \alpha_{AoA}^{q}) \tag{6}$$

The MIMO H-matrix for the q-th MPC can be calculated from equation (7).

$$\mathbf{H}_q = \sqrt{P_q} \begin{bmatrix} e^{j\left(\varphi_q + \Delta\beta_{tx}^{q}(1) + \Delta\beta_{rx}^{q}(1) + \Delta\theta_q\right)} & \cdots & e^{j\left(\varphi_q + \Delta\beta_{tx}^{q}(M) + \Delta\beta_{rx}^{q}(1) + \Delta\theta_q\right)} \\ \vdots & \ddots & \vdots \\ e^{j\left(\varphi_q + \Delta\beta_{tx}^{q}(1) + \Delta\beta_{rx}^{q}(N) + \Delta\theta_q\right)} & \cdots & e^{j\left(\varphi_q + \Delta\beta_{tx}^{q}(M) + \Delta\beta_{rx}^{q}(N) + \Delta\theta_q\right)} \end{bmatrix} \tag{7}$$

where P_q, φ_q and $\Delta\theta_q$ represent the ray power, the point source predicted initial phase, and the uniformly distributed random phase for the q-th traced MPC. Using this procedure we are able to generate a set of MIMO channel matrices with realistic spatial, temporal and spectral correlations that are based on the ray tracing data and the array geometries. Since a deterministic space-time channel model is used, no prior statistical assumptions are required. The resulting H-matrices can now be used as an alternative to the SUI reference model.

III. Channel Analysis

There are six defined SUI channel models (SUI-I to SUI-VI) for the three most common terrain environments (terrain types A to C). Category A is defined as hilly terrain with moderate-to-heavy tree densities. Category C is defined as mostly flat terrain with light tree densities. Category B lies between terrain types A and C. The SUI models define several major channel parameters (such as the K-factor, power delay profile, power Doppler profile, antenna correlations etc). This data assumes that the BS uses a 120^0 directional antenna and that it is mounted 30m above the ground. The CPE is mounted at roof-top height and can be either omni-directional, or use a 30^0 directional antenna pattern. Compared to the SUI model, our RTD-MIMO channel model can work at any deployment height and with any set of antenna patterns. The RTD-MIMO model also provides a wider range of SCM modelling information. Furthermore, there is no need to categorize the environment, since terrain, building and foliage information is inherent in the geographic database.

Figure 3. Section of the Geographic map (central Bristol)

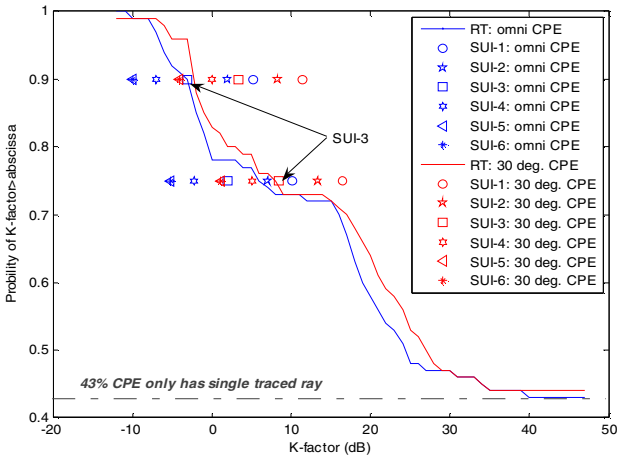

Figure 4. Channel K-factor distribution

Our operating scenario covers a 3 km by 1.8 km region of central Bristol, as shown in Fig. 3. Fig. 4 demonstrates the distribution of the channel K-factor for our deployment. Results demonstrate that 73% of CPEs have very strong LoS (K-factor above 15dB) and 43% of CPEs have a single dominant ray. We see that the K-factor increases when we move from an omni-directional CPE antenna to a correctly aligned 30^0 directional antenna. Analysis of the ray-tracing results indicates that our simulation area fits most closely to the SUI-3 model (assuming terrain type B) for the majority of parameters. However, for the SIMO case it is interesting to note that the spatial correlation from the MIMO-RTD model does not agree with this particular SUI model. SUI models have been implemented for a 1x2 SIMO channel, and these are derived from the application of a correlation matrix **R**. Within the correlation matrix, the diagonal coefficients are identical (and equal to 1). The two off-diagonal coefficients are also assumed to be equal and their value is defined as part of the SUI model configuration (values range from 0.7 down to 0.3 for SUI-1 to SUI-6). For this assumption to hold, the BS and CPE need to be located in a similar environment. The same spatial correlation matrix **R** is then applied to the SIMO fading samples for each delay tap in the tapped delay line model.

Fig. 5 indicates that the RMS Angle Spread (AS) is not identical at the BS and CPE (this is particularly true of the elevation spread). Analysis of the ray tracing results demonstrates that the RMS AS is much lower in elevation, compared with azimuth. This means that there will be higher spatial correlation between vertical displaced array elements, compared to horizontally spaced array elements. Consequently, when deploying MIMO it is more effective to space the elements in the horizontal plane.

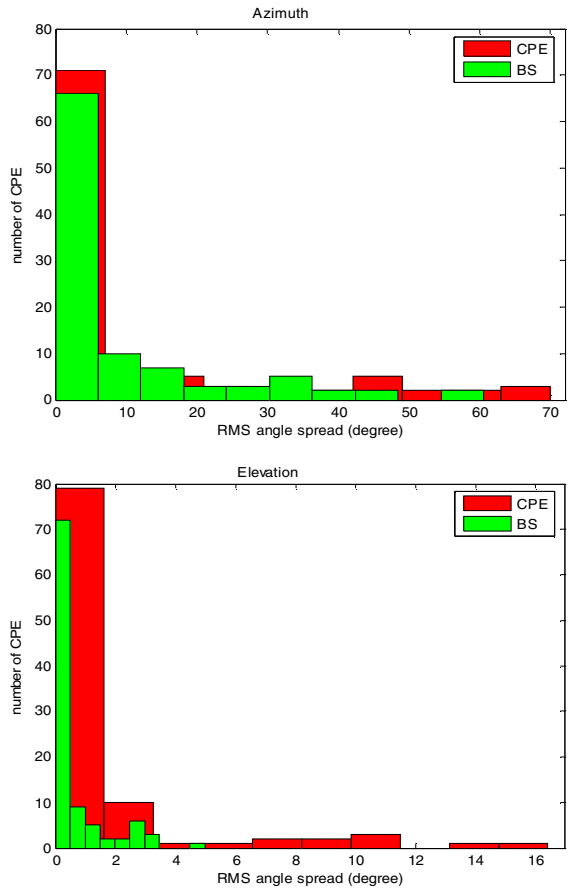

Figure 5. RMS angle spread in azimuth and elevation at BS and CPE

When MIMO is used to exploit diversity gain, the degree of improvement is related to the spatial correlation. For strongly correlated channels, the channel capacity and the diversity gain will degrade. Fig. 6 shows the spatial correlation for the ULA and UCA geometries for a 4x4 MIMO system. The antenna separations are normalized to the wavelength. The Reciprocal Condition Number (RCN) [8] of the MIMO H-matrix is used as a metric to quantify the degree of spatial channel correlation. RCN is computed as the ratio $\min(\mu^2)/\max(\mu^2)$, where μ represents a vector of the singular values of H. If the *RCN* has a value of 1 then the MIMO channels are spatially uncorrelated. In all other cases, the MIMO channels are spatial correlated. Results in fig. 6 indicate that for narrow inter-element spacings the UCA results in higher RCN values (compared to the ULA). When larger inter-element separations are used, the ULA is then able to offer higher RCN values.

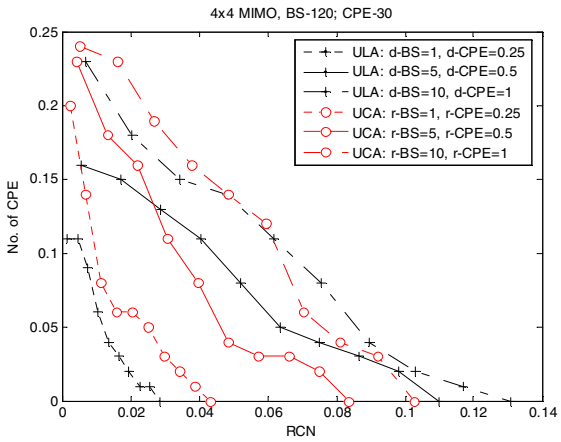

Figure 6. Correlation of ULA and UCA for 4x4 MIMO channels

When systems operate in the presence of CCI there is a trade-off between interference suppression (using narrow beamwidth elements) and diversity gain (where wider beamwidths help to reduce the spatial correlation). If no prior channel knowledge is available at the transmitter then the theoretic channel capacity (bits/s/Hz) for a MIMO-OFDM system can be written as [9]:

$$C \approx \frac{1}{N_f}\sum_{j=1}^{N_f}\log_2 \det\left(I_M + \frac{SINR}{N}\mathbf{H}_j\mathbf{H}_j^H\right) \qquad (8)$$

where *SINR* and N_f represent the signal to interference plus noise ratio and the number of subcarriers respectively. Since we are modelling an OFDM waveform, the distribution of the interference envelope is complex Gaussian. This allows us to consider the interference as an additional noise term in equation (8). $\mathbf{H}_j$ (M by N) represents the frequency response of the MIMO H-matrix for the j-th subcarrier and $(.)^H$ denotes the Hermitian function. The *SINR* is given by

$$SINR = P_{rx}(dBm) - 10\times\log_{10}(P_{\text{int}} + K_{Boltsmann}TB\times NF) \qquad (9)$$

where $K_{Boltsmann} = 1.38\times10^{-20}$ mW per Hz per degrees Kelvin. T, B and NF represent the temperature (in degrees Kelvin), the bandwidth (in Hz) and the noise figure of the receiving unit. P_{rx} and P_{int} denotes the received signal power and interference power in mW. P_{rx} can be computed from the incoherent power sum of all arriving MPCs at a given location. Downlink (DL) interference is generated from all other sectors (including those of other BS) that operate on the same frequency.

IV. Simulation Results

5 BS are now deployed on tall local buildings (with heights greater than 30 m where possible). The centre cell is denoted as BS1, while the four surrounding BS are denoted BS2~5. The surrounding cells produce inter-cell interference into the centre cell. 100 CPEs are distributed at rooftop level (e.g. at heights of around 6 m) over the geographic area. We assume FDD operation with three 120^0 sectors at each BS. Each sector is assigned a unique frequency; however these are then reused in the surrounding BS. With this radio resource assignment there is no intra-cell interference. Fig. 7 illustrates the CPE-BS-sector assignment (using the method described in section II). The Effective Isotropic Radiated Power (EIRP) at each BS was 32 dBm (based on a 8 dBi gain sector antenna).

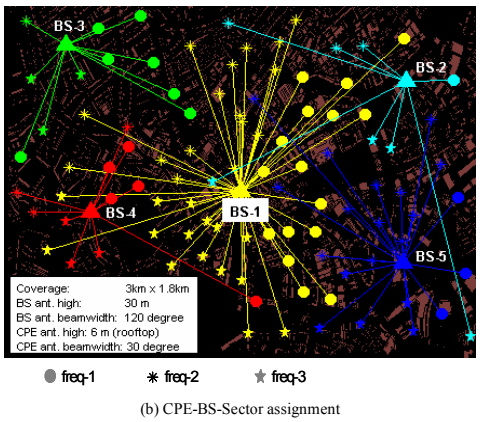

(b) CPE-BS-Sector assignment

Figure 7. Multi-BS system coverage over central of Bristol (3 km by 1 km)

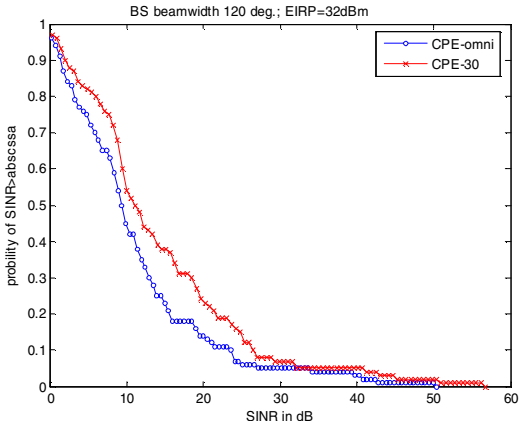

Figure 8. Interference reduction by sectorised antenna at CPE (SISO system)

The system noise temperature was 289 degrees Kelvin and a noise figure of 5 dB was assumed. For our scenario the CCI experienced on the DL at the CPE is far greater than the thermal noise, and hence the deployment is interference limited. Fig. 8 shows that by employing a 30^0 directional antenna at the CPE, the SINR is increased by 2dB assuming an 80% coverage level, and 8dB assuming a 25% coverage level. This occurs since the interference dominates the noise and the narrow CPE beamwidth now rejects CCI from directions away from the wanted link.

The use of a sectorised antenna can actually decrease the AS compared to an omni antenna. This may impact on the suitability of MIMO for 802.16 deployments. The BS often has a smaller AS compared to the CPE, and hence can suffer more from high spatial correlation. To address this, an inter-element array separation of 5 wavelengths was used at the BS. An inter-element spacing of 0.5 wavelengths was used at the CPE

(where a compact unit was required). As discussed in section III, all elements were spaced in the horizontal plane. For the 2x2 MIMO Alamouti scheme, the average SNR at each receiver antenna is improved by a factor of 2 over a SISO link [9]. At each location, the theoretic capacity is determined from equation (8) using the SINR and $\mathbf{HH}^{H}$.

We use the MIMO H-matrix derived from Section II together with the SINR as derived from Section III to calculate the theoretic capacity for every BS-CPE link in the network. Using a 5MHz bandwidth, we then compute the peak data rate and map it to the appropriate coding and modulation scheme in Table 1. We assume that 192 of the 256 carriers are used for data transfer. A COFDM guard interval of 1/4 is selected and the resulting extended OFDM symbol period is 55.5 µs. The peak bit rate under these assumptions for each of the seven 802.16-2004 modes is shown in Table 1.

TABLE I. MODEL DEFINED PARAMETERS AND PEAK THROUGHPUT

Mode	Coding and modulation	Coded bits per sub-carrier	Coded bits per OFDM symbol	Data bits per OFDM symbol	Peak bit rate, Mbps
0	½ BPSK	1	192	96	1.73
1	½ QPSK	2	384	192	3.46
2	¾ QPSK	2	384	288	5.19
3	½ 16QAM	4	768	384	6.92
4	¾ 16QAM	4	768	576	10.3
5	2/3 64QAM	6	1152	768	13.84
6	¾ 64QAM	6	1152	864	15.57

Fig. 9 demonstrates that by using a sectorised 2x2 MIMO array we can improve the rooftop coverage in our urban environment relative to the SISO case. The use of BS sectorisation and directional CPE antennas enables a reasonable level of coverage in the SISO case. It is important to note that these results assume the reuse of all sector frequencies in the neighboring BS. For the MIMO case, we see a theoretic 12% improvement in the coverage of the highest throughput mode (3/4 rate 64QAM). This gain results from the increase in the wanted signal level after Alamouti processing (this gain does not apply to the noise like interference waveforms).

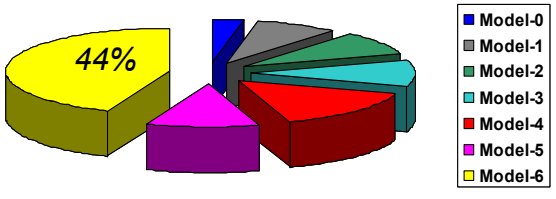

(a) SISO

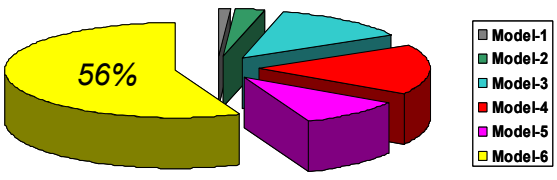

(b) MIMO

Figure 9. Coverage versus capacity for system with link adaption

V. CONCLUSIONS

In this paper, the performance of the IEEE 802.16d WiMAX standard has been analysed for a sectorised system with and without MIMO processing. Channel data was derived from a site specific ray tracing tool based on central Bristol. A complete BS-CPE-sector assignment was performed for 5 BS, each with 3 sectors. Several major channel parameters were computed from the ray-tracing data sets and then compared with the SUI reference model. Our MIMO-RTD model was able to analyse problems without the need to make assumptions on antenna heights, patterns and operating environments. Ray tracing results indicated that MIMO arrays should be deployed in the horizontal plane. MIMO spatial correlation was explored for ULA and UCA geometries. For narrow element spacings (e.g., 0.5 wavelengths) the UCA resulted in lower spatial correlation than the ULA. For wider spacings, the ULA was marginally superior. In the presence of co-channel interference a trade off was noted between interference suppression (using narrow beamwidth elements) and diversity gain (where a wider beamwidth helps to reduce the spatial correlation). We recommend the use of wide MIMO element spacings at the BS (5 wavelengths), with narrow spacings (0.5 wavelengths) at the CPE. Finally, coverage to a large number of CPEs was studied and the most appropriate modulation and coding mode was chosen based on power, inference and spatial correlation. For our test environment, results showed that the sectorised 2x2 MIMO system improved the coverage of the highest link speed by 12% (relative to a SISO system).

ACKNOWLEDGMENT

This work was funded by the British Office of Communications (Ofcom) and Toshiba Telecommunications Research Laboratory (TRL). The authors would like to thank Dr Eustace Tameh for developing and supporting the deterministic propagation model. They would also like to thank Professor M. Beach and Dr. C. Williams for their valuable technical inputs.

REFERENCES

[1] IEEE Std 802.16™-2004, "Part 16: Air interface for fixed broadband wireless access systems," Oct. 2004.

[2] A. Ghosh, D. Wolter, J. Andrew and R. Chen, "Broadband wireless access with WiMAX/802.16: Current performance benchmarks and future potential," *IEEE Commnications Magazine*, Vol. 43, No. 2, Feb. 2005, pp.129-136.

[3] C. Ball, E. Humburg, K. Ivanov and F. Tremi, "Performance analysis of IEEE802.16 based cellular MAN with OFDM-256 in mobile scenarios," *IEEE VTC 2005-spring*, Vol. 3, pp. 2061-2065, May 2005.

[4] IEEE 802.16a-03/01, "Channel models for fixed wireless applications," Jun. 2003.

[5] E. Tameh, A. Nix and M. Beach, "A 3-D integrated macro and microcellular propation model, based on the use of photogram metric terrain and building data," *IEEE VTC1997-spring*, Vol.3, pp.1957-1961, May 1997.

[6] ETSI EN302.326-3 V1.1.1, "Fixed radio systems multipoint equipment and antennas; Part 3: Harmonized EN covering the essential requirements of article 3.2 of the R&TTE directive for multipoint radio antennas," Oct. 2005.

[7] J. Tsai, R. Buehrer and B. Woerner, "BER performance of a uniform circulat array versus a uniform linear array in a mobile radio environment," *IEEE Trans.* On *Wireless Commun.*, Vol. 3, pp. 695-700, May 2004.

[8] V. Nangia, K. Baum, "Ecpermental broadband OFDM system: field resuls for OFDM and OFDM with frequency domain spreading," *IEEE VTC2002-fall.* Vol. 1, pp. 223-227, Sep. 2002.

[9] A. Paulraj, R. Nabar and D. Gore, *Introduction to space-time wireless communications.* Cambridge university press, 2003.